

Strain effects on the spin-orbit induced band structure splittings in monolayer MoS₂ and graphene.

Tawinan Cheiwchanchamnangij and Walter R. L. Lambrecht
Department of Physics, Case Western Reserve University, Cleveland, OH 44106-7079

Yang Song¹ and Hanan Dery^{1,2}

¹*Department of Physics and Astronomy,* ²*Department of Electrical and Computer Engineering,*
University of Rochester, Rochester, New York, 14627

The strain effects on the spin-orbit induced splitting of the valence band maximum and conduction band minimum in monolayer MoS₂ and the gap in graphene are calculated using first-principles calculations. The dependence of these splittings on the various symmetry types of strain is described by means of an effective Hamiltonian based on the method of invariants and the parameters in the model are extracted by fitting to the theory. These splittings are related to acoustic phonon deformation potentials, or electron-phonon coupling matrix elements which enter the spin-dependent scattering theory of conduction in these materials.

PACS numbers: 73.22.Pr 73.30.+y 62.25.-g 73.22.-f

I. INTRODUCTION

Graphene and monolayer MoS₂ are both interesting materials for spin-dependent electronic devices.^{1,2} In spite of their similarities, they also have significant differences. As is well known, graphene has a linear dispersion near the Dirac points and has inversion symmetry. MoS₂ has a gap of about 1.8 eV and the absence of inversion symmetry in monolayer MoS₂ leads to an interesting relation of the spins and the valley degrees of freedom. Both valence band and conduction band edges in the K and K' valleys of the Brillouin zone are split purely by spin-orbit coupling. Because of the time-reversal symmetry between $\psi_{\mathbf{k}\sigma}$ and $\psi_{-\mathbf{k}-\sigma}$, the up and down spin states in opposing valleys are reversed. This relation leads to the possibility of valley control of the carriers by means of circularly polarized excitation.³⁻⁷ On the other hand, spin transport in this material depends on the intra-valley and inter-valley scattering, which arises from the electron-phonon coupling. As is also well known in graphene, ripples play an important role in 2D materials.⁸ These ripples are governed by out-of-plane long-wavelength phonon distortion; the so-called flexural acoustic mode. This mode is associated with the dynamic out-of-plane shear strain. Thus, by studying the splittings and shifts of the energy bands with strain, it is possible to extract deformation potential constants that set the amplitudes of various electron-phonon scattering processes.⁹⁻¹¹ The present study is motivated by this connection.

Strain induced changes in the band gap of MoS₂ have been the subject of several recent papers.¹²⁻¹⁷ The emphasis of those papers is on the strain engineering of the band structure. While we will also present some results on the band gaps with strain, our emphasis is on studying the effect of different types of strain on the band edge spin-orbit splittings in MoS₂. Closely related, the spin-orbit coupling in graphene leads to the opening of a gap

at the Dirac point.¹⁸ The size of this spin-orbit coupling induced gap in graphene is extremely small and has been somewhat controversial with different estimates resulting from different tight-binding models and first-principles calculations.¹⁹⁻²² Here, we present first-principles calculations of this spin-orbit induced gap, and from its dependence on strain we recover the scattering constant for intrinsic spin flips in graphene.⁹ This connection is made via a new strain term that we introduce to the K -point effective Hamiltonian in graphene.

In the theory of electron-phonon scattering, absolute deformation potentials of individual bands play a role.²³⁻²⁵ The so-called absolute hydrostatic deformation potentials lead to shifts of the bands and cannot be extracted from a single bulk calculation because the reference potential in a periodic crystal is ill-defined.²⁶⁻²⁸ An interface calculation is needed between a strained and unstrained region in order to obtain the dipole potential alignment between the two and hence the absolute shifts of the bands. On the other hand, splitting of the bands due to traceless components of the strain tensor are obtainable from a single unit cell calculation, appropriately strained. In this paper, we focus only on deformation potentials which can be extracted from band splittings. It also means that we cannot obtain inter-valley matrix elements in this manner. In spite of these restrictions, the present study should be of interest, because the splittings studied under strain are in principle also directly observable experimentally.

Before embarking on the theory we note that it may be surprising that the spin-orbit splitting would depend on strain at all. After all, the spin-orbit coupling is a relativistic effect resulting mostly from the inner parts of the atom and hence be mostly an atomic property. However, the strain affects the mixing of different atomic orbitals (e.g., different Mo- d orbitals and S- p orbitals in the eigenstates), and as a result the effective splitting does depend measurably on strain. While these effects

are indeed rather small, they present a challenge to the computational accuracy. Nevertheless, systematic errors of density functional theory in its usual local density approximation cancel out in these energy differences (band splittings) and differences of differences (strain induced changes in the splittings). This fact makes it possible to calculate the splittings as long as a sufficiently accurate basis set is used to find the eigenvalues of the crystal potential (i.e., the band structure). The all-electron linearized band structure methods like the full-potential linearized muffin-tin orbital method (FP-LMTO) satisfies the requirements.

The plan of the paper is as follows. In Sec. II we derive effective Hamiltonian forms using the method of invariants. In Sec. III we present details of the first-principles computational method employed. In Sec. IV, we present the first-principles results on the splittings under the effect of different types of strain. These results confirm the strain dependence of the splittings on strain as predicted by the effective Hamiltonian models. The parameters of these models are then obtained by fitting the strain dependence to the calculated curves. For the importance of these parameters in the description of the spin-dependent relaxation processes, we refer the reader to Ref. [9].

II. THEORY

The dependence of spin-orbit coupling induced splitting on strain is governed by an effective Hamiltonian describing only the states near this splitting as function of different strain components. To obtain the forms of these effective Hamiltonians, we employ the method of invariants.^{23,25,29–31} This group theoretical framework provides the terms allowed by symmetry. Simply put, the strain tensor is decomposed in irreducible representations of the point group of the \mathbf{k} -point where the band splitting of interest occurs. The Hamiltonian must belong to the fully symmetric irreducible representation (IR). Group theory thus determines which terms, linear or quadratic in the strain component, are allowed in the Hamiltonian. In the case of MoS₂, the states near the splitting are determined by a 2×2 Hamiltonian while in the case of graphene, the Dirac cone is represented by a 4×4 Hamiltonian, including both the orbital pseudospin and real spin degrees of freedom. The theory thus predicts linear or quadratic dependence of the band splittings on different types of strain.

A. MoS₂ effective Hamiltonian

In the absence of strain, the spin-orbit split states at the K -point band edges in MoS₂ are described by a 2×2 matrix, conveniently expressed in terms of the Pauli matrices and unit matrix:

$$H_0 = \bar{E}\mathbf{1} + \frac{1}{2}\Delta_0\sigma_z. \quad (1)$$

Here \bar{E} is the average of up and down spin bands without spin-orbit splitting and as an arbitrary constant it can be set to zero. Δ_0 is the spin-orbit splitting. The same form applies to the valence band maximum (VBM) and conduction band minimum (CBM) although of course the value of Δ_0 is rather different.³² We distinguish them by means of a subscript v or c for VBM and CBM, respectively. It is much smaller for the CBM ($\Delta_{0c} = 3.36$ meV) than for the VBM ($\Delta_{0v} = 146$ meV) because the CBM states are derived mostly from the Mo- $d_{3z^2-r^2}$ orbital which has quantum number $L_z = 0$, and hence zero spin-orbit coupling. It is only because of the small deviation of the Mo atomic potential from spherical symmetry due to the crystal structure, and because of the small components from S p_x, p_y orbitals that it is not zero.³³ On the other hand, the VBM consists of $d_{x^2-y^2}, d_{xy}$ like states. The strain adds terms $b(\epsilon)$ on the diagonal and $a_i(\epsilon)$ ($i = x, y$) on the off-diagonal of the form

$$H_{strain} = \frac{1}{2}b(\epsilon)\sigma_z + \frac{1}{2}\sum_{i=x,y} a_i(\epsilon)\sigma_i. \quad (2)$$

We employ symmetrized strain-tensor components, $\epsilon_{ij} = (du_i/dx_j + du_j/dx_i)/2$, where u_i is the displacement of the i -th cartesian coordinate.⁴⁴ The strain dependent splitting of $H_0 + H_{strain}$ becomes

$$\Delta(\epsilon) = \sqrt{[\Delta_0 + b(\epsilon)]^2 + |a(\epsilon)|^2}. \quad (3)$$

Next, we specify the dependence of $b(\epsilon)$ and $a(\epsilon)$ for different symmetry components of the strain tensor. The flexural modes or out-of-plane strain-tensor components (ϵ_{xz} and ϵ_{yz}) are odd with respect to the mirror-plane passing through the MoS₂ layer. Accordingly, they can only contribute even terms to the diagonal and odd terms to the off-diagonal parts of the effective Hamiltonian. Hence, to lowest non-zero order,

$$a_i(\epsilon_{iz}) \approx a_1\epsilon_{iz}, \quad b(\epsilon_{iz}) \approx b_2\epsilon_{iz}^2. \quad (4)$$

Contrary to the out-of-plane case, in-plane strain components ($\epsilon_{xx}, \epsilon_{yy}, \epsilon_{xy}$) are even with respect to the horizontal mirror-plane. The off-diagonal terms must necessarily be zero and cannot lead to spin-flip scattering,⁹ whereas the leading diagonal term is linear in strain,

$$a_i(\epsilon_{ij}) = 0, \quad b(\epsilon_{ij}) \approx b_1\epsilon_{ij} + b_2\epsilon_{ij}^2 + \dots \quad (5)$$

For the VBM under out-of-plane strain ϵ_{iz} , the zero strain splitting is large compared to the strain terms and one might thus think that the term $b_2\epsilon_{iz}^2$ may be entirely neglected. In that case expanding the square root, one obtains

$$\Delta_v(\epsilon_{iz}) = \Delta_{0v} + \frac{a_{1v}^2\epsilon_{i,z}^2}{2\Delta_{0v}}, \quad (6)$$

which predicts a quadratic increase of the spin-orbit splitting with strain. However, we find that the splitting actually decreases. This implies that $b_2\epsilon_{iz}^2$ cannot be

neglected and has negative b_{2v} because it is the only contribution that can reduce the splitting. So keeping this important term, we can write

$$\Delta_v(\epsilon_{iz})^2 = \Delta_{0v}^2 + (a_{1v}^2 + 2b_{2v}\Delta_0)\epsilon_{iz}^2 + b_{2v}^2\epsilon_{iz}^4. \quad (7)$$

For the CBM and out-of-plane strain, the zero-strain splitting is much smaller so that the strain may become dominant and give rise to a linear strain dependence,

$$\Delta_c(\epsilon) \approx |a_{1c}|\epsilon_{iz} \quad (8)$$

except for very small strains, where it should still look quadratic.

Turning to in-plane strains, there are no off-diagonal terms and the leading term is linear in strain, so we simply have

$$\Delta_c(\epsilon_{ij}) = \Delta_{0c} + b_{1c}\epsilon_{ij} + b_{2c}\epsilon_{ij}^2. \quad (9)$$

However, the b_{1c} for ϵ_{xy} vanishes, in which case the dependence is again quadratic on strain. In Appendix A, we derive this exact cancelation of b_{1c} for ϵ_{xy} , and also the analytical expression of b_{1c} for ϵ_{ii} . The latter is shown to result from competition between first and second order perturbation terms. For the conduction band, where the spin-orbit splitting is small, the linear in strain term turns out to be also small for tensional strain in the plane. Thus, the quadratic term can become dominant for sufficiently large strains. We will see that in fact b_{2c} is negative in that case.

B. Graphene effective Hamiltonian

To write the strain-dependent Hamiltonian in graphene, we invoke the transformation properties of the states and strain tensor in its K point. This information is summarized in Table IV (Appendix B). The states in the edges of the conduction and valence bands of the Dirac point transform as Γ_7 and Γ_9 . Each of these two-dimensional IRs reflects the sublattice orbital degeneracy (pseudospin) and real spin degeneracy due to the space inversion symmetry.³¹ Table IV also includes invariants that tell us that the coupling between the edge states and strain can be written in the following Hamiltonian form

$$H = \begin{pmatrix} a(\epsilon) + \frac{\Delta_D}{2} & 0 & b(\epsilon) & ic(\epsilon) \\ 0 & a(\epsilon) + \frac{\Delta_D}{2} & ic^*(\epsilon) & b^*(\epsilon) \\ b^*(\epsilon) & -ic(\epsilon) & a(\epsilon) - \frac{\Delta_D}{2} & 0 \\ -ic^*(\epsilon) & b(\epsilon) & 0 & a(\epsilon) - \frac{\Delta_D}{2} \end{pmatrix}. \quad (10)$$

Δ_D is the strain independent gap induced by spin-orbit coupling.¹⁸ This gap separates the edge states of the conduction and valence bands in the Dirac point. The diagonal strain term, $a(\epsilon)$, is an hydrostatic deformation potential that merely shifts the Dirac point relative to the average electrostatic potential. Its magnitude scales with the local changes in the density of electrons in response to

contraction or dilatation of the unit-cell.^{8,34} The connection with strain components follows the transformation properties of the identity IR (Γ_1),

$$a(\epsilon) = \Xi_d [(\epsilon_{xx} + \epsilon_{yy}) - \frac{1}{2}(\epsilon_{xz}^2 + \epsilon_{yz}^2)]. \quad (11)$$

The hydrostatic term comprises linear (quadratic) components of in-plane (out-of-plane) strain. These terms share a single deformation potential constant (Ξ_d) because graphene has only one atomic layer; unlike MoS₂ which has some intrinsic thickness, in undistorted graphene all atoms lie in the same plane. This fact means that a flexural strain ($\epsilon_{xz}, \epsilon_{yz}$) can be viewed as a mere stretch of the membrane. Using elementary geometry, it is readily seen that $\epsilon_{xz}^2/2$ or $\epsilon_{yz}^2/2$ correspond to ϵ_{xx} or ϵ_{yy} . To represent this physics, we also use $\epsilon_{iz} = \partial u_z / \partial x_i$ to define the out-of-plane tensor component in graphene.

Contrary to the diagonal strain term, the off-diagonal terms in Eq. (10) affect the size of the gap according to

$$E_g = \sqrt{\Delta_D^2 + 4|b(\epsilon)|^2 + 4|c(\epsilon)|^2}. \quad (12)$$

$b(\epsilon)$ and $c(\epsilon)$ are shear-strain components that couple the edge states ($\Gamma_7 \times \Gamma_9 = \Gamma_5 + \Gamma_6$). The coupling between states of similar spin possesses Γ_6 symmetry, and its form reads

$$b(\epsilon) = \Xi_o \left[\epsilon_{xx} - \epsilon_{yy} + 2i\epsilon_{xy} - \frac{\epsilon_{xz}^2 - \epsilon_{yz}^2 + 2i\epsilon_{xz}\epsilon_{yz}}{2} \right]. \quad (13)$$

Again, we may see that this coupling comprises linear (quadratic) components of in-plane (out-of-plane) strain. The spin-independent deformation potential constant, Ξ_o , is often described by means of a fictitious vector potential due to changes in the hopping energy between nearest neighbor orbitals.^{8,34-36} Importantly, as shear strain does not change the unit-cell area to leading order, this parameter is not associated with local changes in the density of electrons. Hence, it can be calculated via density functional theory in the local density approximation.

Compared with previous works,^{8,34-36} our contribution to the strain Hamiltonian of graphene is the spin-orbit coupling term in the anti-diagonal of Eq. (10). It possesses Γ_5 symmetry due to the coupling between states of opposite spin, and its form reads

$$c(\epsilon) = c_{so}(\epsilon_{yz} + i\epsilon_{xz}). \quad (14)$$

Contrary to the spin-independent terms, this term comprises linear out-of-plane strain. We will make use of this feature to extract its magnitude. The importance of the spin-orbit coupling deformation potential constant, c_{so} , is realized from the fact that it is directly related to the intrinsic spin relaxation in graphene.⁴⁵

Putting these pieces together, the change of the gap in response to pure in-plane strain becomes

$$E_g = \sqrt{\Delta_D^2 + 4\Xi_o^2[(\epsilon_{xx} - \epsilon_{yy})^2 + 4\epsilon_{xy}^2]}. \quad (15)$$

Similarly, the change of the gap in response to pure out-of-plane strain becomes

$$E_g = \sqrt{\Delta_D^2 + \Xi_o^2 (\epsilon_{xz}^2 + \epsilon_{yz}^2) + 4c_{so}^2 (\epsilon_{yz}^2 + \epsilon_{xz}^2)}. \quad (16)$$

In the following, we will use Eqs. (15) and (16) to determine the corresponding shear deformation potential parameters Ξ_o and c_{so} by fitting to first-principles calculations including appropriate strain combinations.

III. COMPUTATIONAL METHOD

Density functional theory is used in the local density approximation following the von-Barth-Hedin parametrization. The band structures are calculated using the full-potential linearized muffin-tin orbital (FP-LMTO) method as described in Refs. [37] and [38]. A double (κ, R_{sm}) basis set is used, including *spdf* and *spd* for the first and second set respectively. Here, $\kappa^2 = E - v_{mtz}$ represents the kinetic energy of the smoothed Hankel function, or its decay length, while the R_{sm} is a smoothing radius (See Bott *et al.* in Ref. [39]). Brillouin zone integrations are carried out using a $13 \times 13 \times 3$ and $14 \times 14 \times 7$ k-point sets for graphene and MoS₂, respectively. Augmentation is carried out inside the muffin-tin-spheres up to $l_{max} = 4$.

The LDA underestimates the gap significantly in MoS₂,³² but for the changes in the splitting considered here, it is sufficient to consider the quasiparticle self-energy shift to be independent of strain. Similarly, in graphene the LDA underestimates the Fermi velocity or slope of the Dirac cone. Using the quasiparticle-self-consistent *GW* method,⁴⁰ we obtain a change of the Dirac cone slope from $0.8 \pm 0.1 \times 10^6$ m/s in LDA to $1.1 \pm 0.1 \times 10^6$ m/s in good agreement with van Schilfgaarde and Katsnelson.⁴¹ For the present purposes of deriving the strain dependent deformation potentials, the LDA results are deemed sufficiently accurate.

IV. RESULTS

A. MoS₂

Figure 1a shows the splitting of the valence band as a function of out-of-plane strain. As already mentioned, the splitting decreases as function of strain. The fitted parameters to Eq. (7) are $a_{1v} = 573$ meV and $b_{2v} = -2.42$ eV. Figure 1b shows the splitting of the conduction band as a function of out-of-plane strain. We can see that it behaves nearly linear for sufficiently large strain. The parameters were obtained by directly fitting the square-root behavior and resulted in $a_{1c} = 774$ meV and $b_{2c} = 263$ meV.

Next, we consider the in-plane strains. As predicted in Eq. (9) for ϵ_{xy} with vanishing b_1 , both VBM and CBM splittings are quadratic in ϵ_{xy} . This behavior is shown

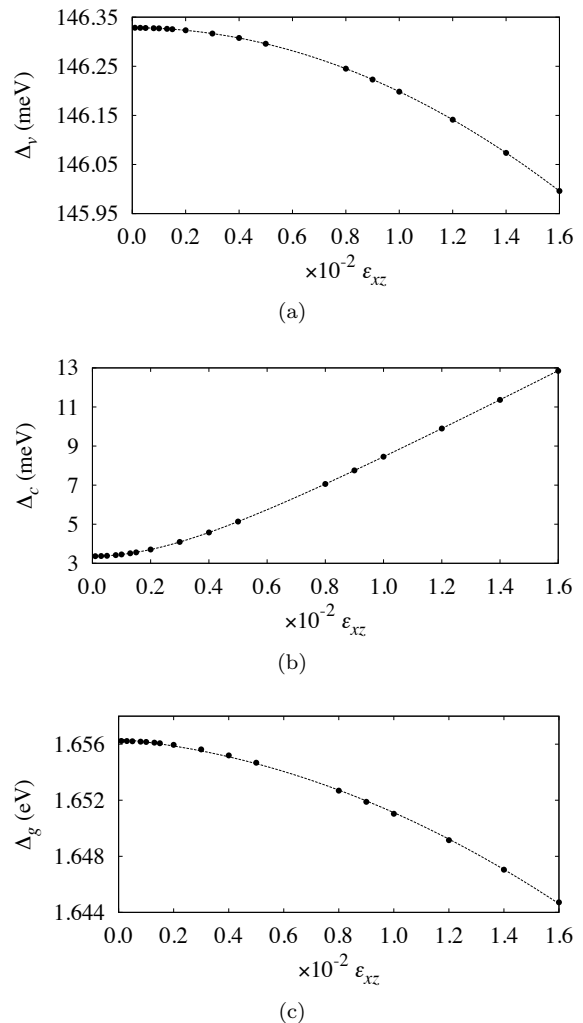


FIG. 1: (a) valence band splitting, (b) conduction band splitting, and (c) band gap of monolayer MoS₂ as a function of out-of-plane strain (ϵ_{xz})

in Figs. 3a and 3b. By fitting Eq. (9) to the calculated data, b_2 parameters are found to be -2.67 eV and -3.45 eV for VBM and CBM, respectively. In case of tensile strain (ϵ_{xx}), the splitting for both VBM and CBM show the combination of linear and quadratic in ϵ_{xx} characters. However, the positive linear coefficient (b_1) of VBM, which is 115 meV, is more than ten times larger than the one for the CBM, which is 8.85 meV. In contrast, their negative quadratic coefficients (b_2), -1.92 eV for the VBM and -1.81 eV for the CBM, are of the same order of magnitude. Therefore, the fit of the VBM splitting in Fig. 2a is dominated by the linear term while the fit of CBM splitting in Fig. 2b is quickly dominated by the quadratic term when ϵ_{xx} is larger than 0.001. Furthermore, the CBM splitting goes through a maximum as function of in-plane tensile strain. All of the parameters mentioned above are tabulated in Table I.

We also consider the gaps as function of strain in Figs. 1c, 2c, and 3c. Band gaps as function of strain are fitted

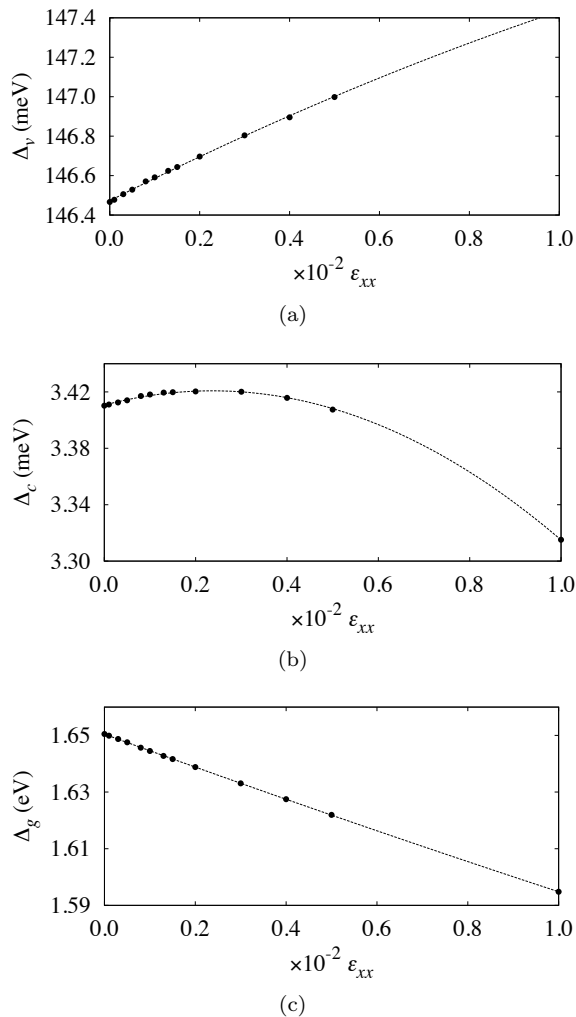


FIG. 2: (a) valence band splitting, (b) conduction band splitting, and (c) band gap of monolayer MoS₂ as a function of tensile strain (ϵ_{xx})

with a quadratic function

$$\Delta_g(\epsilon) = \Delta_g^0 + c_1\epsilon + c_2\epsilon^2, \quad (17)$$

and the resulting parameters are summarized in Table II. We can see that the tensile in-plane strain ϵ_{xx} has a much stronger effect on the band gap than the shear strains. The linear decrease of the gap of about 59 meV/% strain is close to the calculated value reported by Conley *et al.*⁴² The quadratic terms however are not negligible for the shear strains and seem to be of similar magnitude for each strain although it is negative for out of plane strain and positive for in-plane strain.

B. Graphene

First, we note that we obtain a spin-orbit induced gap at the Dirac point of about 26 μeV in the absence of strain. This result is in good agreement with the linearized augmented plane wave (LAPW) calculations by

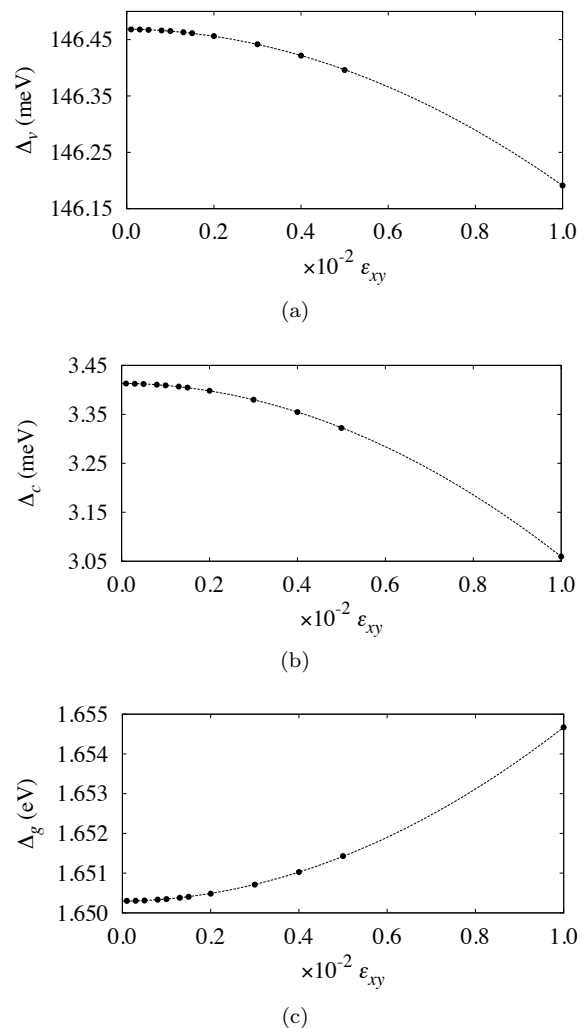


FIG. 3: (a) valence band splitting, (b) conduction band splitting, and (c) band gap of monolayer MoS₂ as a function of in-plane strain (ϵ_{xy})

TABLE I: Parameters for monolayer MoS₂

Strain	Parameter	VBM	CBM
$\epsilon_{xz}, \epsilon_{yz}$	a_1	573 meV	774 meV
	b_2	-2.42 eV	263 meV
$\epsilon_{xx}, \epsilon_{yy}$	b_1	115 meV	8.58 meV
	b_2	-1.92 eV	-1.81 eV
ϵ_{xy}	b_2	-2.67 eV	-3.45 eV
	Δ_0	146 meV	3.36 meV

Gmitra *et al.*²¹ In Fig. 4 we show the gap squared as function of strain squared for in-plane and out-of-plane strain. Different in-plane strains, ϵ_{xx} , $\epsilon_{xx} - \epsilon_{yy}$, ϵ_{xy} gave somewhat different results for the extracted fitting parameters because of numerical effects. We use these to estimate the uncertainty on the extracted parameters, given in Table III. In a separate Figure 5 we show the small strain behavior as function of ϵ_{xx} and as function

TABLE II: Parameters for the change in band gap of mono-layer MoS₂

Strain	c_1	c_2
ϵ_{xz}	-175 meV	-34.9 eV
ϵ_{xx}	-5.87 eV	30.5 eV
ϵ_{xy}	13.5 meV	42.4 eV

of ϵ_{yz}^2 , which clearly shows that there is no linear spin-orbit term for the in-plane strain case but only for the out-of-plane strain case. We note that for strains of the order of 0.001, the c_{so} term is comparable in magnitude with the Ξ_o term. The linear fit in the small strain region gives an uncertainty of about 8% on the slope parameter or on c_{so} .

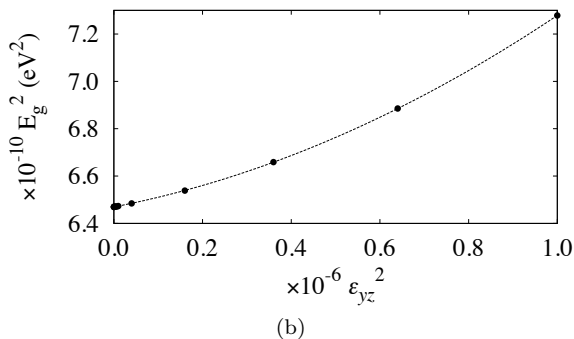
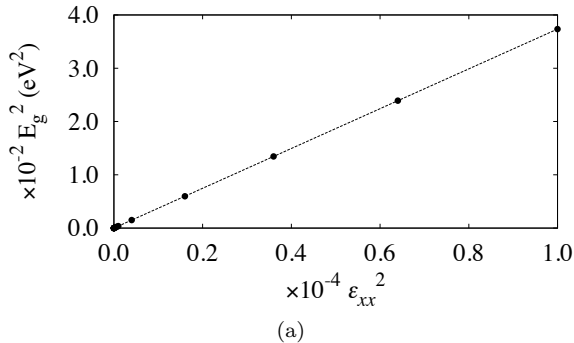


FIG. 4: Band gap squared with spin-orbit-coupling effect of graphene at K -point as function of (a) ϵ_{xx} , and (b) ϵ_{yz} strain squared

TABLE III: Parameters obtained from fittings for graphene.

Δ_D (μeV)	Ξ_o (eV)	c_{so} (meV)
26 ± 1	9.5 ± 0.5	2.9 ± 0.3

V. CONCLUSIONS

The strain-dependent spin splittings of MoS₂ and graphene are systematically studied. The spin-orbit induced splittings of the valence-band maximum,

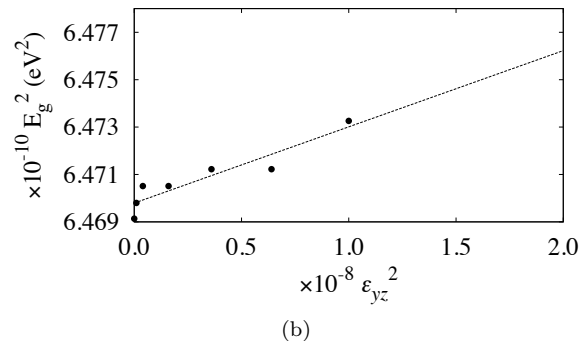
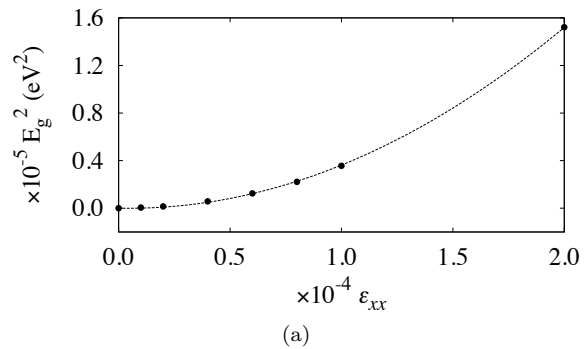


FIG. 5: Band gap squared of graphene at K -point as function of (a) ϵ_{xx} , and (b) ϵ_{yz}^2 for small strains.

conduction-band minimum and the gap in MoS₂ as well as the spin-orbit induced gap in graphene were studied as function of strain using first-principles calculations. Various spin-dependent and spin-independent deformation potentials were extracted, in comparison with strain Hamiltonians governed by the method of invariants. The importance of these deformation potentials is that they directly dictate the strength of intrinsic spin-flip and momentum scattering due to electron-phonon interaction. The obtained spin-dependent deformation potential for graphene $c_{so} \approx 3$ meV, rather than the much smaller Dirac gap ($\sim 26 \mu\text{eV}$), is the important parameter in studying the intrinsic spin relaxation in graphene. Similarly, sizable spin-dependent deformation potentials on the order of atomic spin-orbit coupling ($\gtrsim 0.1$ eV) render strong electron spin relaxation in MoS₂, despite the tiny spin splitting in its conduction band minimum (~ 3.4 meV).

Acknowledgments

The calculations made use of the High Performance Computing Resource in the Core Facility for Advanced Research Computing at Case Western Reserve University. The work at CWRU was supported by NSF under grant DMR-1104595. The work at the University of Rochester was supported by NRI-NSF, NSF, and DTRA Contracts No. DMR-1124601, No. ECCS-1231570, and No. HDTRA1-13-1-0013, respectively.

Appendix A: Detailed derivation of in plane spin-dependent deformations of MoS₂

The expressions of b_1 in Eq. (9) are obtained through perturbation theory and method of invariants. The general perturbation brought by in-plane strain is

$$\begin{aligned}
H_{strain}^{in} &= \sum_{i,j=\{x,y\}} r_i \frac{\partial V}{\partial r_j} \epsilon_{ij} \\
&= \frac{1}{2} \left(x \frac{\partial V}{\partial x} + y \frac{\partial V}{\partial y} \right) (\epsilon_{xx} + \epsilon_{yy}) \\
&\quad + \frac{1}{2} \left(x \frac{\partial V}{\partial y} - y \frac{\partial V}{\partial x} \right) (\epsilon_{xy} - \epsilon_{yx}) \\
&\quad + \frac{1}{4} \left[\left(x \frac{\partial V}{\partial x} - y \frac{\partial V}{\partial y} \right) + i \left(x \frac{\partial V}{\partial y} + y \frac{\partial V}{\partial x} \right) \right] \\
&\quad \times [(\epsilon_{xx} - \epsilon_{yy}) - i(\epsilon_{xy} + \epsilon_{yx})] \\
&\quad + \frac{1}{4} \left[\left(x \frac{\partial V}{\partial x} - y \frac{\partial V}{\partial y} \right) - i \left(x \frac{\partial V}{\partial y} + y \frac{\partial V}{\partial x} \right) \right] \\
&\quad \times [(\epsilon_{xx} - \epsilon_{yy}) + i(\epsilon_{xy} + \epsilon_{yx})], \quad (A1)
\end{aligned}$$

where the first two terms both transform as K_1 which is the identity irreducible representation (IR) of the K -point C_{3h} group.⁹ The last two terms transform as $K_{2,3}$ IRs. For simplicity, we have omitted the $p_i p_j \epsilon_{ij} / m$ terms in H_{strain}^{in} (they transform the same as $r_i \partial V / \partial r_j$). Using the one-dimension nature of all the IRs in C_{3h} ($K_i \times K_i^* = K_1$), intra-band coupling via the invariants $(\epsilon_{xx} + \epsilon_{yy})\sigma_z$ or $(\epsilon_{xy} - \epsilon_{yx})\sigma_z$ is symmetry-allowed in all of the bands. The corresponding integral constant of this intra-band coupling comes from second-order perturbation (one due to strain and another due to spin-orbit) as well as from first-order perturbation (strain-modified spin-orbit interaction). Below, we show that the two parts cancel-out partially for a general integral constant associated with $\epsilon_{ij}\sigma_z$ of spin-independent band K_n . The first-order perturbation part due to strain-modified spin-orbit interaction reads

$$\begin{aligned}
&\lambda \langle K_n | [\nabla (r_i \frac{\partial V}{\partial r_j}) \times \mathbf{p}]_z | K_n \rangle \\
&+ \lambda \langle K_n | -\delta_{xi} \frac{\partial V}{\partial r_j} p_y + \delta_{yi} \frac{\partial V}{\partial r_j} p_x | K_n \rangle \\
&+ \lambda \langle K_n | -\delta_{yi} \frac{\partial V}{\partial x} p_j + \delta_{xi} \frac{\partial V}{\partial y} p_j | K_n \rangle \\
&= \lambda \langle K_n | r_i \frac{\partial (\nabla \times \mathbf{p})_z}{\partial r_j} | K_n \rangle + \\
&\quad \lambda \langle K_n | (-\delta_{yi} \frac{\partial V}{\partial x} + \delta_{xi} \frac{\partial V}{\partial y}) p_j | K_n \rangle, \quad (A2)
\end{aligned}$$

where $\lambda = \hbar / 4m_0^2 c^2$. Eq. (A2) assumes rigid-ion approximation, but it retains the correct symmetry and does not

affect the result qualitatively. The second-order perturbation part reads,

$$\frac{2\text{Re} \left[\langle K_n | \left(r_i \frac{\partial V}{\partial r_j} + \frac{p_i p_j}{m} \right) \sum_{n'} | K_{n'} \rangle \langle K_{n'} | \lambda (\nabla \times \mathbf{p})_z | K_n \rangle \right]}{E_{K_n} - E_{K_{n'}}}, \quad (A3)$$

where $K_{n'}$ is other bands at K point excluding the K_n band. Using the fact that $\frac{\partial V}{\partial r_j} = [p_j, H]$, we get that

$$\begin{aligned}
&\frac{2\text{Re} \left[\langle K_n | r_i \frac{\partial V}{\partial r_j} \sum_{n'} | K_{n'} \rangle \langle K_{n'} | \lambda (\nabla \times \mathbf{p})_z | K_n \rangle \right]}{E_{K_n} - E_{K_{n'}}} \\
&= \frac{2}{\hbar} \text{Im} \left[\langle K_n | r_i p_j \sum_{n'} | K_{n'} \rangle \langle K_{n'} | \lambda (\nabla \times \mathbf{p})_z | K_n \rangle \right]. \quad (A4)
\end{aligned}$$

Dispensing with the identity operator altogether, we get

$$\begin{aligned}
&-\frac{i}{\hbar} \langle K_n | r_i p_j \lambda (\nabla \times \mathbf{p})_z - \lambda (\nabla \times \mathbf{p})_z r_i p_j | K_n \rangle \\
&= -\lambda \langle K_n | r_i \frac{\partial (\nabla \times \mathbf{p})_z}{\partial r_j} | K_n \rangle \\
&\quad + \lambda \langle K_n | (\delta_{yi} \frac{\partial V}{\partial x} - \delta_{xi} \frac{\partial V}{\partial y}) p_j | K_n \rangle. \quad (A5)
\end{aligned}$$

This term cancels out the first-order perturbation part [Eq. (A2)], and the net result from adding Eqs. (A2) and (A3) is

$$\frac{2\text{Re} \left[\langle K_n | \frac{p_i p_j}{m} \sum_{n'} | K_{n'} \rangle \langle K_{n'} | \lambda (\nabla \times \mathbf{p})_z | K_n \rangle \right]}{E_{K_n} - E_{K_{n'}}}. \quad (A6)$$

Therefore, by Eq. (A1) and the argument that followed it, the integral constant $b_{1,z}$ associated with shear strain drops ($p_y p_x - p_x p_y = 0$), while the integral constant associated with dilation strain remains ($p_x p_x + p_y p_y \neq 0$). In practice, $\epsilon_{xy} - \epsilon_{yx}$ is treated as 0 since rotation does not induce energy perturbation, and the accompanied deformation potentials are not evaluated. The above derivation justifies this practice from the detailed interaction Hamiltonian, while Eq. (A6) times two gives the detailed expression for b_1 with $i = j$.

Finally, when $|K_n\rangle$ is dominated by orbitals with zero angular momentum (e.g., lowest conduction band of MoS₂), the majority of b_1 vanishes, since $(\nabla \times \mathbf{p})_z |d_{z^2}\rangle = 0$. So b_1 is small in this case and is proportional to the small components from S p_x, p_y orbitals,³³ and the small deviation of the Mo atomic potential from spherical symmetry due to the crystal structure.⁹

Appendix B: Character tables and invariants

TABLE IV: Character table of the D_{3h} point double group.⁴³ It is used to construct the strain-dependent Hamiltonian in the K point of graphene. $\{x, y, z\}$ and $\{R_x, R_y, R_z\}$ represent components of a polar and axial vectors, respectively. The x -axis is defined along the zigzag edge direction and the y -axis is along the armchair direction. A strain tensor component ϵ_{ij} transforms as the product of the i -th and j -th components of a polar-vector.

D_{3h}	E	\bar{E}	C_3^+	C_3^-	\bar{C}_3^+	\bar{C}_3^-	σ_h	$\bar{\sigma}_h$	S_3^+	S_3^-	\bar{S}_3^+	\bar{S}_3^-	C_{2i}^+	\bar{C}_{2i}^-	σ_{vi}	$\bar{\sigma}_{vi}$	invariants
$A_1' \Gamma_1$	1	1	1	1	1	1	1	1	1	1	1	1	1	1	1	1	$z^2, x^2 + y^2, x(3y^2 - x^2)$
$A_2' \Gamma_2$	1	1	1	1	1	1	1	1	1	1	1	-1	-1	-1	-1	-1	$R_z, y(3x^2 - y^2)$
$A_1'' \Gamma_3$	1	1	1	1	-1	-1	-1	-1	-1	-1	-1	1	1	1	1	1	
$A_2'' \Gamma_4$	1	1	1	1	-1	-1	-1	-1	-1	-1	-1	1	1	1	1	1	z
$E'' \Gamma_5$	2	2	-1	-1	-2	1	1	0	0	0	0	0	0	0	0	0	$\{R_x, R_y\}, \{yz, -xz\}$
$E' \Gamma_6$	2	2	-1	-1	2	-1	-1	0	0	0	0	0	0	0	0	0	$\{x, y\}, \{x^2 - y^2, -2xy\}$
$\bar{E}_1 \Gamma_7$	2	-2	1	-1	0	$\sqrt{3}$	$-\sqrt{3}$	0	0	0	0	0	0	0	0	0	$\{\uparrow_z, \downarrow_z\}, \{iR_x - R_y \downarrow_z, iR_x + R_y \uparrow_z\}$
$\bar{E}_2 \Gamma_8$	2	-2	1	-1	0	$-\sqrt{3}$	$\sqrt{3}$	0	0	0	0	0	0	0	0	0	
$\bar{E}_3 \Gamma_9$	2	-2	-2	2	0	0	0	0	0	0	0	0	0	0	0	0	$\{iR_x + R_y \downarrow_z, iR_x - R_y \uparrow_z\}$

TABLE V: Character table of the C_{3h} point double group.⁴³ It is used to construct the strain-dependent Hamiltonian in the K point of MX_2 . The function notations are defined in the same way as in Table IV.

C_{3h}	E	C_3^+	C_3^-	σ_h	S_3^+	S_3^-	\bar{E}	\bar{C}_3^+	\bar{C}_3^-	$\bar{\sigma}_h$	\bar{S}_3^+	\bar{S}_3^-	invariants
$A' K_1$	1	1	1	1	1	1	1	1	1	1	1	1	$R_z, x^2 + y^2, z^2$
${}^2E' K_2$	1	ω	ω^*	1	ω	ω^*	1	ω	ω^*	1	ω	ω^*	$x - iy, 2xy - i(x^2 - y^2)$
${}^1E' K_3$	1	ω^*	ω	1	ω^*	ω	1	ω^*	ω	1	ω^*	ω	$x + iy, 2xy + i(x^2 - y^2)$
$A'' K_4$	1	1	1	-1	-1	-1	1	1	1	-1	-1	-1	z
${}^2E'' K_5$	1	ω	ω^*	-1	$-\omega$	$-\omega^*$	1	ω	ω^*	-1	$-\omega$	$-\omega^*$	$R_x - iR_y, yz + ixz$
${}^1E'' K_6$	1	ω^*	ω	-1	$-\omega^*$	$-\omega$	1	ω^*	ω	-1	$-\omega^*$	$-\omega$	$R_x + iR_y, yz - ixz$
${}^1\bar{E}_3 K_7$	1	$-\omega$	$-\omega^*$	i	$-i\omega$	$i\omega^*$	-1	ω	ω^*	$-i$	$i\omega$	$-i\omega^*$	\uparrow_z
${}^2\bar{E}_3 K_8$	1	$-\omega^*$	$-\omega$	$-i$	$i\omega^*$	$-i\omega$	-1	ω^*	ω	i	$-i\omega^*$	$i\omega$	\downarrow_z
${}^2\bar{E}_2 K_9$	1	$-\omega$	$-\omega^*$	$-i$	$i\omega$	$-i\omega^*$	-1	ω	ω^*	i	$-i\omega$	$i\omega^*$	
${}^1\bar{E}_2 K_{10}$	1	$-\omega^*$	$-\omega$	i	$-i\omega^*$	$i\omega$	-1	ω^*	ω	$-i$	$i\omega^*$	$-i\omega$	
${}^1\bar{E}_1 K_{11}$	1	-1	-1	i	$-i$	i	-1	1	1	$-i$	i	$-i$	
${}^2\bar{E}_1 K_{12}$	1	-1	-1	$-i$	i	$-i$	-1	1	1	i	$-i$	i	

$$\omega = \exp(2\pi i/3).$$

¹ H. Dery, H. Wu, B. Ciftcioglu, M. Huang, Y. Song, R. Kawakami, J. Shi, I. Kivrorotov, and L. J. Sham, IEEE Tran. Electron Device. **59**, 259 (2012).

² Z. Gong, G.-B. Liu, H. Yu, D. Xiao, X. Cui, X. Xu, and W. Yao, Nature Comm. **4**, 2053 (2013).

³ W. Feng, Y. Yao, W. Zhu, J. Zhou, W. Yao, and D. Xiao, Phys. Rev. B **86**, 165108 (2012), URL <http://link.aps.org/doi/10.1103/PhysRevB.86.165108>.

⁴ K. F. Mak, K. He, J. Shan, and T. F. Heinz, Nature Nanotec. **7**, 494 (2012).

- ⁵ H. Zeng, J. Dai, W. Yao, D. Xiao, and X. Cui, *Nature Nanotech.* **7**, 490 (2012).
- ⁶ G. Kioseoglou, A. T. Hanbicki, M. Currie, A. L. Friedman, D. Gunlycke, and B. T. Jonker, *Appl. Phys. Lett.* **101**, 221907 (2012), URL <http://dx.doi.org/10.1063/1.4768299>.
- ⁷ G. Sallen, L. Bouet, X. Marie, G. Wang, C. R. Zhu, W. P. Han, Y. Lu, P. H. Tan, T. Amand, B. L. Liu, et al., *Phys. Rev. B* **86**, 081301(R) (2012), URL <http://link.aps.org/doi/10.1103/PhysRevB.86.081301>.
- ⁸ A. H. Castro Neto, F. Guinea, N. M. R. Peres, K. S. Novoselov, and A. K. Geim, *Rev. Mod. Phys.* **81**, 109 (2009), URL <http://link.aps.org/doi/10.1103/RevModPhys.81.109>.
- ⁹ Y. Song and H. Dery, *Phys. Rev. Lett.* **111**, 026601 (2013), URL <http://link.aps.org/doi/10.1103/PhysRevLett.111.026601>.
- ¹⁰ K. Kaasbjerg, K. S. Thygesen, and K. W. Jacobsen, *Phys. Rev. B* **85**, 115317 (2012), URL <http://link.aps.org/doi/10.1103/PhysRevB.85.115317>.
- ¹¹ K. Kaasbjerg, K. S. Thygesen, and A.-P. Jauho, *Phys. Rev. B* **87**, 235312 (2013), URL <http://link.aps.org/doi/10.1103/PhysRevB.87.235312>.
- ¹² W. S. Yun, S. W. Han, S. C. Hong, I. G. Kim, and J. D. Lee, *Phys. Rev. B* **85**, 033305 (2012), URL <http://link.aps.org/doi/10.1103/PhysRevB.85.033305>.
- ¹³ E. Scalise, M. Houssa, G. Pourtois, V. Afanas'ev, and A. Stesmans, *Nano Research* **5**, 43 (2012), ISSN 1998-0124, URL <http://dx.doi.org/10.1007/s12274-011-0183-0>.
- ¹⁴ P. Lu, X. Wu, W. Guo, and X. C. Zeng, *Phys. Chem. Chem. Phys.* **14**, 13035 (2012).
- ¹⁵ H. Pan and Y.-W. Zhang, *J. Phys. Chem. C* **116**, 11752 (2012).
- ¹⁶ Q. Yue, J. Kang, Z. Shao, X. Zhang, S. Chang, G. Wang, S. Qin, and J. Li, *Phys. Lett. A* **376**, 1166 (2012).
- ¹⁷ H. Peelaers and C. G. Van de Walle, *Phys. Rev. B* **86**, 241401 (2012), URL <http://link.aps.org/doi/10.1103/PhysRevB.86.241401>.
- ¹⁸ C. L. Kane and E. J. Mele, *Phys. Rev. Lett.* **95**, 226801 (2005), URL <http://link.aps.org/doi/10.1103/PhysRevLett.95.226801>.
- ¹⁹ H. Min, J. E. Hill, N. A. Sinitsyn, B. R. Sahu, L. Kleinman, and A. H. MacDonald, *Phys. Rev. B* **74**, 165310 (2006), URL <http://link.aps.org/doi/10.1103/PhysRevB.74.165310>.
- ²⁰ D. Huertas-Hernando, F. Guinea, and A. Brataas, *Phys. Rev. B* **74**, 155426 (2006), URL <http://link.aps.org/doi/10.1103/PhysRevB.74.155426>.
- ²¹ M. Gmitra, S. Konschuh, C. Ertler, C. Ambrosch-Draxl, and J. Fabian, *Phys. Rev. B* **80**, 235431 (2009), URL <http://link.aps.org/doi/10.1103/PhysRevB.80.235431>.
- ²² S. Konschuh, M. Gmitra, and J. Fabian, *Phys. Rev. B* **82**, 245412 (2010), URL <http://link.aps.org/doi/10.1103/PhysRevB.82.245412>.
- ²³ G. L. Bir and G. E. Pikus, *Symmetry and strain-induced effects in semiconductors* (Halsted Press, Jerusalem, 1974), 1st ed.
- ²⁴ M. Cardona and P. Y. Yu, *Fundamentals of Semiconductors* (Springer, 1999), second edition ed.
- ²⁵ Y. Song and H. Dery, *Phys. Rev. B* **86**, 085201 (2012), URL <http://link.aps.org/doi/10.1103/PhysRevB.86.085201>.
- ²⁶ L. Kleinman, *Phys. Rev. B* **24**, 7412 (1981), URL <http://link.aps.org/doi/10.1103/PhysRevB.24.7412>.
- ²⁷ M. Cardona and N. E. Christensen, *Phys. Rev. B* **35**, 6182 (1987), URL <http://link.aps.org/doi/10.1103/PhysRevB.35.6182>.
- ²⁸ C. G. Van de Walle and R. M. Martin, *Phys. Rev. Lett.* **62**, 2028 (1989), URL <http://link.aps.org/doi/10.1103/PhysRevLett.62.2028>.
- ²⁹ J. M. Luttinger, *Phys. Rev.* **102**, 1030 (1956), URL <http://link.aps.org/doi/10.1103/PhysRev.102.1030>.
- ³⁰ R. Winkler, *Spin-Orbit Coupling Effects in Two-Dimensional Electron and Hole Systems* (Springer, Berlin, 2003), 1st ed.
- ³¹ R. Winkler and U. Zülicke, *Phys. Rev. B* **82**, 245313 (2010), URL <http://link.aps.org/doi/10.1103/PhysRevB.82.245313>.
- ³² T. Cheiwchanchamnangij and W. R. L. Lambrecht, *Phys. Rev. B* **85**, 205302 (2012), URL <http://link.aps.org/doi/10.1103/PhysRevB.85.205302>.
- ³³ Z. Y. Zhu, Y. C. Cheng, and U. Schwingenschlögl, *Phys. Rev. B* **84**, 153402 (2011), URL <http://link.aps.org/doi/10.1103/PhysRevB.84.153402>.
- ³⁴ H. Suzuura and T. Ando, *Phys. Rev. B* **65**, 235412 (2002), URL <http://link.aps.org/doi/10.1103/PhysRevB.65.235412>.
- ³⁵ C. L. Kane and E. J. Mele, *Phys. Rev. Lett.* **78**, 1932 (1997), URL <http://link.aps.org/doi/10.1103/PhysRevLett.78.1932>.
- ³⁶ E. V. Castro, H. Ochoa, M. I. Katsnelson, R. V. Gorbachev, D. C. Elias, K. S. Novoselov, A. K. Geim, and F. Guinea, *Phys. Rev. Lett.* **105**, 266601 (2010), URL <http://link.aps.org/doi/10.1103/PhysRevLett.105.266601>.
- ³⁷ M. Methfessel, M. van Schilfhaarde, and R. A. Casali, in *Electronic Structure and Physical Properties of Solids. The Use of the LMTO Method*, edited by H. Dreyssé (Berlin Springer Verlag, 2000), vol. 535 of *Lecture Notes in Physics*, p. 114.
- ³⁸ T. Kotani and M. van Schilfhaarde, *Phys. Rev. B* **81**, 125117 (2010), URL <http://link.aps.org/doi/10.1103/PhysRevB.81.125117>.
- ³⁹ E. Bott, M. Methfessel, W. Krabs, and P. C. Schmidt, *Journal of Mathematical Physics* **39**, 3393 (1998), URL <http://link.aip.org/link/?JMP/39/3393/1>.
- ⁴⁰ T. Kotani, M. van Schilfhaarde, and S. V. Faleev, *Phys. Rev. B* **76**, 165106 (pages 24) (2007), URL <http://link.aps.org/abstract/PRB/v76/e165106>.
- ⁴¹ M. van Schilfhaarde and M. I. Katsnelson, *Phys. Rev. B* **83**, 081409 (2011), URL <http://link.aps.org/doi/10.1103/PhysRevB.83.081409>.
- ⁴² H. J. Conley, N. Wang, J. I. Ziegler, R. F. Haglund, S. T. Pantelides, and K. I. Bolotin (2013), arXiv:1305.3880.
- ⁴³ C. J. Bradley and A. P. Cracknell, *The Mathematical Theory of Symmetry in Solids: Representation Theory for Point Groups and Space Groups* (Clarendon Press, Oxford, 1972), 1st ed.
- ⁴⁴ In Ref. [9] we worked with non-symmetrized forms in which out-of-plane displacements (du_z/dx_i) are treated separately. Therefore, the scattering parameter Ξ_K^{so} in Ref. [9] is to be associated with $a_i/4$ in this work [Eq. (2)].
- ⁴⁵ The relation between c_{so} in this work and the scattering constant Ξ_{so} in Eq. (6) of Ref. [9] is $\Xi_{so} = 2c_{so}$.